We are IntechOpen, the world's leading publisher of Open Access books
Built by scientists, for scientists

5,300
Open access books available

130,000
International authors and editors

155M
Downloads

154
Countries delivered to

Our authors are among the

TOP 1%
most cited scientists

12.2%
Contributors from top 500 universities

CLARIVATE ANALYTICS
BOOK CITATION INDEX
INDEXED

WEB OF SCIENCE™

Selection of our books indexed in the Book Citation Index
in Web of Science™ Core Collection (BKCI)

Interested in publishing with us?
Contact book.department@intechopen.com

Self-Calibration of Precision $XY\theta_z$ Metrology Stages

Chuxiong Hu, Yu Zhu and Luzheng Liu

Abstract

This chapter studies the on-axis calibration for precision $XY\theta_z$ metrology stages and presents a holistic $XY\theta_z$ self-calibration approach. The proposed approach uses an artifact plate, specially designed with XY grid mark lines and angular mark lines, as a tool to be measured by the $XY\theta_z$ metrology stages. In detail, the artifact plate is placed on the uncalibrated $XY\theta_z$ metrology stages in four measurement postures or views. Then, the measurement error can be modeled as the construction of $XY\theta_z$ systematic measurement error (i.e. stage error), artifact error, misalignment error, and random measurement noise. With a new property proposed, redundance of the $XY\theta_z$ stage error is obtained, while the misalignment errors of all measurement views are determined by rigid mathematical processing. Resultantly, a least square-based $XY\theta_z$ self-calibration law is synthesized for final determination of the stage error. Computer simulation is conducted, and the calculation results validate that the proposed scheme can accurately realize the stage error even under the existence of various random measurement noise. Finally, the designed artifact plate is developed and illustrated for explanation of a standard $XY\theta_z$ self-calibration procedure to meet practical industrial requirements.

Keywords: $XY\theta_z$ stage, self-calibration, measurement system, least square, stage error

1. Introduction

Precision $XY\theta_z$ motion stages are ubiquitously utilized in industrial mechanical systems to meet the requirement of high-performance manufacture [1]. As automatical servo systems, these stages have both precision linear encoders and angle encoders for measurement and motion feedback control [2–7]. In practice, the measurement accuracy inevitably suffers from surface non-flatness and un-roundness, axis nonorthogonality, scale graduation nonuniformity, encoder installation eccentricity, read-head misalignment, and so on, which resultantly generate systematic measurement error, i.e. stage error. The stage error can in principle be eliminated through calibration technology [8–10]. Due to the difficulty on finding a more accurate standard tool in traditional calibration technologies, self-calibration technology has been developed with utilization of an artifact with mark positions not precisely known. As an alternative of intelligent calibration processes, self-calibration is an effective and economical approach especially for micro-/nano-level mechanical systems [11–14].

Existing self-calibration technologies were developed for X, XY, XYZ, and angular metrology stages, respectively. For example, Takac studied one-dimensional

self-calibration and developed a scheme that made a set of tool graduation marks appear to have identical spacing with relative scale [15]. In [16], self-calibration method for single-axis dual-drive nanometer positioning stage was presented. In [17], an *XY* self-calibration strategy was presented for two-dimensional metrology stages, which used an artifact plate as assistance measured by three views to construct equations of stage error, misalignment error, and artifact error. Fourier transformation was employed in the scheme to meet the challenge of random measurement noise. This method is popularly followed by many engineers and researchers [18–21]. In [18], a self-calibration algorithm was developed to test the out-of-plane error of two-dimensional profiling stages. The algorithm suppresses artifact-related errors in consideration of the geometrical congruence of three profile measurement views. Computer simulation and experimental results both showed that the calibration accuracy was free from artifact imperfection and only minimally affected by random measurement errors. In [19], a self-calibration method was proposed for mapping the errors in XY plane and the squareness error between Z-axis and XY plane of the scanning probe microscopes. In [22, 23], self-calibration approach for three-dimensional metrology stages was completely provided with experimental validation.

On the other hand, lots of self-calibration technologies have been developed for angular metrology systems [14, 24] in US National Institute of Standards and Technology (NIST), National Metrology Institute of Japan (NMIJ), Germany's National Metrology Institute the Physikalisch-Technische Bundesanstalt (PTB), Korea Research Institute of Standards and Science, etc. Specifically, circle closure principle was frequently used to cross-calibrate index tables in NIST [25, 26]. A high-precision rotary encoder self-calibration system was built based on equal-division-averaged method and had been adopted as the angular national standard system in NMIJ [27, 28]. The equal-division-averaged method was also expanded for self-calibration of the scale error in an angle comparator [29]. In addition, a known prime factor algorithm-based method was presented for self-calibration of divided circles in PTB [30, 31].

In summary of previous self-calibration strategies, a systematic self-calibration strategy for calibration of $XY\theta_z$ metrology stage is seldom published up to present. To address this problem, we have proposed a preliminary framework to self-calibrate the $XY\theta_z$ stage error in [32], assuming that the angular coordinate and the XY coordinate are uncorrelated while the XY stage error and θ_z stage error are solved separately. This assumption leads to the final $XY\theta_z$ calibration being not in a uniform coordinate, which means that it is not a complete and accurate $XY\theta_z$ self-calibration strategy. In this chapter, we further study the self-calibration of precision $XY\theta_z$ metrology stages and present a complete and accurate on-axis self-calibration approach. Specifically, a new artifact plate is designed as the assistant tool, and four measurement views of the designed artifact plate on the uncalibrated $XY\theta_z$ metrology stage are constructed to provide measurement information. The detailed specification of the artifact plate on the $XY\theta_z$ stage is shown in **Figure 1**. Combining with symmetry, transitivity, and circle closure principle, certain redundance of the $XY\theta_z$ stage error is established, while the misalignment errors of all measurement views are determined by rigid mathematical manipulation. Resultantly, a least square-based $XY\theta_z$ self-calibration law is proposed for the final determination of the stage error. Computer simulation is conducted, and the calculation results validate that scheme proposed in this paper can figure out the stage error rather accurately in the absence of random measurement noise. The self-calibration accuracy of the proposed scheme is also tested to meet the challenge of various random measurement noises, and the calibration results validate that the scheme can effectively alleviate the effects of random measurement noise. Finally, the
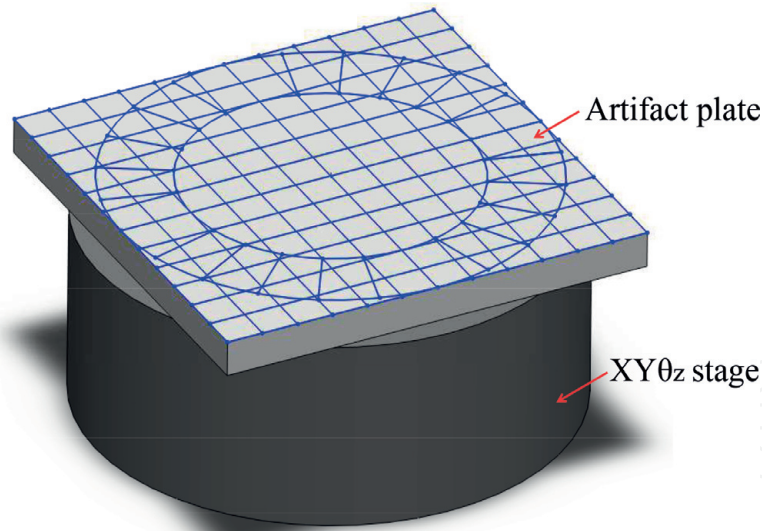
Figure 1.
An artifact plate with mark lines on an XYθ_z metrology stage.

designed artifact plate is manufactured, and a standard on-axis $XY\theta_z$ self-calibration procedure following the proposed scheme is introduced.

The proposed scheme mainly features the following two benefits: (1) Departing from previous self-calibration technologies, the proposed scheme first solves the on-axis self-calibration problem of $XY\theta_z$ metrology stages and (2) complicated mathematical manipulations, especially the calculations of misalignment errors in previous XY self-calibration schemes, are significantly avoided in the proposed strategy. The remainder of this chapter is organized as follows. In Section II, the stage error of $XY\theta_z$ metrology stage is explained, and a newly designed artifact plate and related artifact error are also described. The principle of the developed $XY\theta_z$ self-calibration scheme with four measurement views is presented in Section III. In Section IV, computer simulation is conducted to show the calibration performance of the proposed method. And the procedure for performing a standard $XY\theta_z$ self-calibration is presented in Section V. Finally, the conclusion is provided in Section VI.

2. Self-calibration problem formulation

2.1 Stage error

For a $XY\theta_z$ metrology system, linear encoders are employed for measuring movement along X and Y axes, and a rotary encoder for measuring rotation along θ_z axis. Thus, the systematic errors along X-axis, Y-axis, and θ_z axis are independent. And once the metrology system is set, the geometric relationship among X-axis, Y-axis, and θ_z axis is also determined, which will be described in detail later. In the Cartesian grid, define $\mathbf{G}_l(x,y)$ as the linear stage error at (x,y) where (x,y) is the true location. And $\mathbf{G}_r(\theta_z)$ is the rotary stage error at θ_z where θ_z is the true angle value. Herein, the uncalibrated $XY\theta_z$ field consists of XY with $L \times L$ and θ_z with $360°$, while the $XY\theta_z$ origin point is set as the same at the center of the $L \times L$ field. In the following, we define

$$\mathbf{G}_l(x,y) \equiv G_x(x,y)\mathbf{e}_x + G_y(x,y)\mathbf{e}_y$$
$$\mathbf{G}_r(\theta_z) \equiv G_{\theta_z}(\theta_z)\mathbf{e}_{\theta_z}$$

(1)

where $\mathbf{e}_x$, $\mathbf{e}_y$, and $\mathbf{e}_{\theta_z}$ are the unit vectors of the stage axes. For notation, we combine linear and rotary stage errors and define $\mathbf{G}(x,y,\theta_z)$ is the stage error at (x,y,θ_z) where (x,y) is the true location and θ_z is the true angle in the Cartesian grid:

$$\begin{aligned}\mathbf{G}(x,y,\theta_z) &\equiv \mathbf{G}_l(x,y) + \mathbf{G}_r(\theta_z) \\ &= G_x(x,y)\mathbf{e}_x + G_y(x,y)\mathbf{e}_y + G_{\theta_z}(\theta_z)\mathbf{e}_{\theta_z}\end{aligned} \quad (2)$$

Suppose the X-Y sample sites are in an $N \times N$ square array (N is odd) covering the $L \times L$ field and the θ_z sample lines are in a K array (K is a multiple of 4) covering the 360° field. Then in the Cartesian grid, the positions of the sample sites are

$$x_m = m\Delta, y_n = n\Delta, \theta_k = k\ominus \quad (3)$$

where $m = -\frac{N-1}{2}, -\frac{N-3}{2}, ..., \frac{N-1}{2}$, $n = -\frac{N-1}{2}, -\frac{N-3}{2}, ..., \frac{N-1}{2}$, and $\Delta = L/N$ which is called sample site interval; $k = 0, 1, 2, ..., K-1$ and $\ominus = 360/K°$. For notation simplicity, through Eq. (2), we can denote

$$\mathbf{G}_{m,n,k} \equiv G_{x,m,n}\mathbf{e}_x + G_{y,m,n}\mathbf{e}_y + G_{\theta_z,k}\mathbf{e}_{\theta_z} \quad (4)$$

where $G_{\theta_z,k} \equiv G_{\theta_z}(\theta_k)$, $G_{x,m,n} \equiv G_x(x_m,y_n)$, and $G_{y,m,n} \equiv G_y(x_m,y_n)$.

Similar to the detailed explanation in [17], to define the coordinates' origin, orientation, and grid scale of the XY axes stage, there are no translation property, no rotation property, and no magnification property for $G_{x,m,n}$ and $G_{y,m,n}$, which can be expressed mathematically as

$$\begin{aligned}&\sum_{m,n} G_{x,m,n} = \sum_{m,n} G_{y,m,n} = 0 \\ &\sum_{m,n}\left(G_{y,m,n}x_m - G_{x,m,n}y_n\right) = 0 \\ &\sum_{m,n}\left(G_{x,m,n}x_m + G_{y,m,n}y_n\right) = 0\end{aligned} \quad (5)$$

For X-Y axes, two dimensionless parameters O and R are defined as the XY nonorthogonality and the XY scale difference of $G_{x,m,n}$ and $G_{y,m,n}$, respectively. As a result, $G_{x,m,n}$ and $G_{y,m,n}$ are

$$\begin{aligned}G_{x,m,n} &= Oy_n + Rx_m + F_{x,m,n} \\ G_{y,m,n} &= Ox_m - Ry_n + F_{y,m,n}\end{aligned} \quad (6)$$

Therefore, one can obtain $G_{x,m,n}$ and $G_{y,m,n}$ by the first calculation of the first-order components O and R, and the later determination of the residual error $F_{x,m,n}$ and $F_{y,m,n}$. Noting that the origin of XY axes is the center of the sample array, we also can get the following properties of $F_{x,m,n}$ and $F_{y,m,n}$ which is also detailed in [17, 20]:

$$\begin{aligned}&\sum_{m,n}F_{x,m,n} = \sum_{m,n}F_{x,m,n}x_m = \sum_{m,n}F_{x,m,n}y_n = 0 \\ &\sum_{m,n}F_{y,m,n} = \sum_{m,n}F_{y,m,n}x_m = \sum_{m,n}F_{y,m,n}y_n = 0\end{aligned} \quad (7)$$

Besides, for rotary self-calibration, an important property, i.e. the circle closure principle, could directly bridge the gap between G_{k+K} and G_k, i.e. $G_{k+K} = G_k$ for $k = 0, 1, 2, ..., K-1$, which significantly facilitates the self-calibration process. To calculate the stage error components at θ_z, i.e. $G_{\theta_z,k}$, a new property must be pointed out as follows:

$G_{\theta_z,k}$ is definitely related to the errors of *XY* orientations. In other words, the expected value of angle deviation of points is exactly the θ_z orientation error of the

radius vector where the points lie in. Angle deviation of points here means the angle between position vector of actual point and that of ideal point. Take $G_{\theta_z, 0}$ as an example. For the point $(m, 0)$ on +X-axis, $\left(m = 1, 2, \cdots, \frac{N-1}{2}\right)$, define ϕ_m as the angle deviation of the point $(m, 0)$, i.e.

$$\phi_m = \; <(x_m + G_{x,m,0}, y_0 + G_{y,m,0}), (x_m, y_0)>$$
$$= \; <(x_m + G_{x,m,0}, G_{y,m,0}), (x_m, 0)>$$

where $<\mathbf{a}, \mathbf{b}>$ is the angle between vectors $\mathbf{a}$ and $\mathbf{b}$ and, then,

$$G_{\theta_z, 0} = E(\phi_m)$$

where $E(\phi_m)$ is the expectation of ϕ_m.
Noting that $G_{y,m,0} \ll x_m$ and $G_{x,m,0} \ll x_m$, one can obtain

$$\phi_m = \; <(x_m + G_{x,m,0}, G_{y,m,0}), (x_m, 0)>$$
$$= \arctan\left(\frac{G_{y,m,0}}{x_m + G_{x,m,0}}\right)$$
$$\doteq \arctan\left(\frac{G_{y,m,0}}{x_m}\right)$$
$$\doteq \frac{G_{y,m,0}}{x_m}$$

which subsequently results in

$$G_{\theta_z, 0} = E\left(\frac{G_{y,m,0}}{x_m}\right) \tag{8}$$

Similarly, along X-axis and Y-axis, we can obtain the following four equations:

$$
\begin{aligned}
G_{\theta_z, 0} &= E\left(\frac{G_{y,m,0}}{x_m}\right) & \left(m = 1, 2, \cdots, \frac{N-1}{2}\right) \\
G_{\theta_z, \frac{K}{4}} &= E\left(-\frac{G_{x,0,n}}{y_n}\right) & \left(n = 1, 2, \cdots, \frac{N-1}{2}\right) \\
G_{\theta_z, \frac{K}{2}} &= E\left(\frac{G_{y,m,0}}{x_m}\right) & \left(m = -1, -2, \cdots, -\frac{N-1}{2}\right) \\
G_{\theta_z, \frac{3K}{4}} &= E\left(-\frac{G_{x,0,n}}{y_n}\right) & \left(n = -1, -2, \cdots, -\frac{N-1}{2}\right)
\end{aligned}
\tag{9}
$$

The goal of the proposed self-calibration method is to determine $\mathbf{G}_{m,n,k}$ through different measurement postures, through which the measurement accuracy can be compensated directly.

2.2 Artifact error

In this chapter, an artifact plate which possesses mark lines different from previous researches in [17, 20] is designed specifically for $XY\theta_z$ self-calibration. **Figure 2** shows the details of artifact plate on the stage. In detail, an $N \times N$ grid mark array is on the artifact plate with the same size as the stage sample site array. Furthermore, it has K mark lines with equal angle interval. The plate $XY\theta_z$ coordinate axis' origin is located on the center of the mark array. During the plate

movement, the plate axis will move with the plate. The locations of the nominal mark in the plate coordinate system are totally the same with that of the sample site in the stage coordinate system. Due to the unavoidable imperfection of the artifact plate, all the actual marks at (m, n, k) deviate from their nominal location by $\mathbf{A}_{m,n,k}$ which is defined as artifact error expressed by

$$
\mathbf{A}_{m,n,k} \equiv A_{x,m,n}\mathbf{e}_{px} + A_{y,m,n}\mathbf{e}_{py} + A_{\theta_z,k}\mathbf{e}_{pz}
$$
$$
A_{x,m,n} \equiv A_x(x_m, y_n), A_{y,m,n} \equiv A_y(x_m, y_n), \tag{10}
$$
$$
A_{\theta_z,k} \equiv A_{\theta_z}(\theta_k)
$$

where $m = -\frac{N-1}{2}, -\frac{N-3}{2}, ..., \frac{N-1}{2}$, $n = -\frac{N-1}{2}, -\frac{N-3}{2}, ..., \frac{N-1}{2}$, and $k = 0, 1, ..., K-1$; $\mathbf{e}_{px}$, $\mathbf{e}_{py}$, and $\mathbf{e}_{pz}$ are the unit vectors of the plate axes.

It should be noted that every mark on the artifact plate has an identification number (m, n, k). During the motions of the plate on the stage, the identification number of the mark will not change. This characteristic is also utilized to identify each physical mark of the plate in the following comparison of different measurement views. $A_{x,m,n}$ and $A_{y,m,n}$ also have no translation property and no rotation property [17, 20], which essentially have defined the axis origin and axis orientation, i.e.

$$
\sum_{m,n} A_{x,m,n} = \sum_{m,n} A_{y,m,n} = 0
$$
$$
\sum_{m,n} (A_{y,m,n}x_m - A_{x,m,n}y_n) = 0 \tag{11}
$$

3. $XY\theta_z$ self-calibration principle

3.1 The measurement views

The self-calibration method is based on four different postures or views of the designed artifact plate on the uncalibrated $XY\theta_z$ metrology stage, which is shown in **Figure 3**. As shown in **Figure 3**, the $XY\theta_z$ stage is the gray part, while the artifact plate is the white part. The 3-D specification can also be found in **Figures 1** and **2**.

Without the loss of generality, for each view, there inevitably exists a misalignment error; for that these coordinate axes cannot be aligned completely,
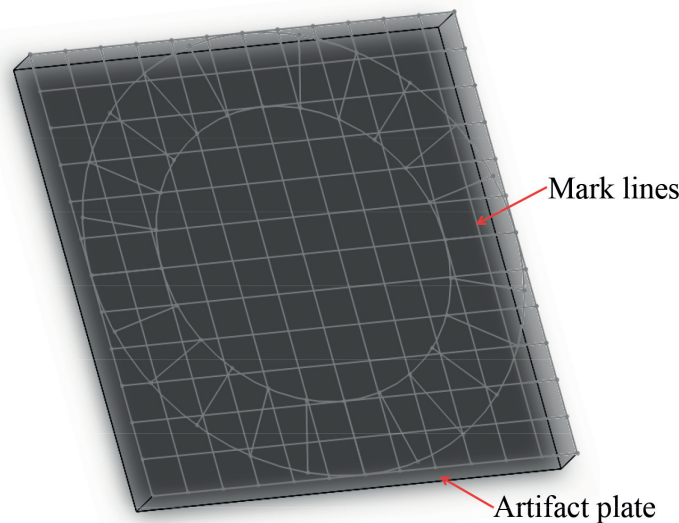
Figure 2.
A designed artifact plate with mark lines for $XY\theta_z$ self-calibration.

which will be considered as a misalignment error, which consists of a small rotation between their orientations and a small offset between their origins. Besides, random measurement noise also exists in the measurement process, but the effects of noise can be assumed to be completely attenuated by repeated measurements:

a. In View 0, which is the initial view, the *XYθ$_z$* axes of the plate are aligned as closely in line with those of the stage as possible; in this view, both grid and angular marks are measured.

b. In View 1, the artifact plate is rotated 90°, around the origin from View 0 on the stage; in this view, both grid and angular marks are measured.

c. In View 2, the artifact plate is rotated 360/*K*°, i.e., ⊖, around the origin from View 0 on the stage; in this view, only angular marks are measured.

d. In View 3, the artifact plate is translated by one sample site, i.e., Δ, along +X-axis from View 0 on the stage; in this view, both grid and angular marks are measured.

For each measurement view, the artifact plate is firmly fixed on the stage, and a mark alignment system is needed to help the *XYθ$_z$* metrology stage to precisely measure the mark lines. The detailed instruments are presented later.

In the following, we would present the measurement and mathematical manipulations of each measurement view and then the reconstruction of the stage error map, in which *V* stands for the measured deviation for a mark from its nominal position in the stage coordinate.
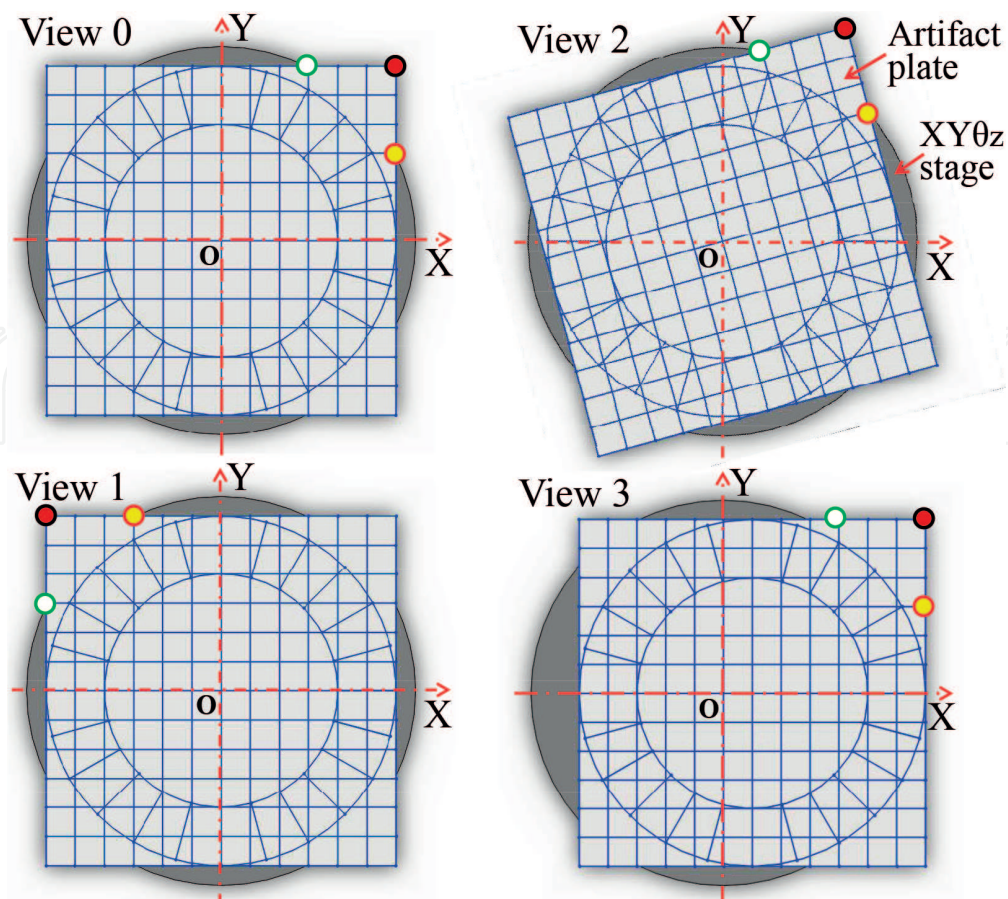

Figure 3.
Independent measurement views for XYθ$_z$ self-calibration.

For View 0,

$$V_{0,x,m,n} = G_{x,m,n} + A_{x,m,n} - \varphi_0 y_n + t_{0x}$$

$$V_{0,y,m,n} = G_{y,m,n} + A_{y,m,n} + \varphi_0 x_m + t_{0y} \tag{12}$$

$$V_{0,\theta_z,k} = G_{\theta_z,k} + A_{\theta_z,k} + \varphi_0$$

where $m = -\frac{N-1}{2}, -\frac{N-3}{2}, ..., \frac{N-1}{2}$, $n = -\frac{N-1}{2}, -\frac{N-3}{2}, ..., \frac{N-1}{2}$, and $k = 1, 2, ..., K$.
For View 1,

$$V_{1,x,m,n} = G_{x,-n,m} - A_{y,m,n} - \varphi_1 x_m + t_{1x}$$

$$V_{1,y,m,n} = G_{y,-n,m} + A_{x,m,n} - \varphi_1 y_n + t_{1y} \tag{13}$$

$$V_{1,\theta_z,k} = G_{\theta_z,k+\frac{K}{4}} + A_{\theta_z,k} + \varphi_1$$

where $m = -\frac{N-1}{2}, -\frac{N-3}{2}, ..., \frac{N-1}{2}$, $n = -\frac{N-1}{2}, -\frac{N-3}{2}, ..., \frac{N-1}{2}$, and $k = 1, 2, ..., K$.
For View 2,

$$V_{2,\theta_z,k} = G_{\theta_z,k+1} + A_{\theta_z,k} + \varphi_2 \tag{14}$$

where $k = 1, 2, ..., K$.
For View 3,

$$V_{3,x,m,n} = G_{x,m+1,n} + A_{x,m,n} - \varphi_3 y_n + t_{3x}$$

$$V_{3,y,m,n} = G_{y,m+1,n} + A_{y,m,n} + \varphi_3 x_m + t_{3y} \tag{15}$$

$$V_{3,\theta_z,k} = G_{\theta_z,k} + A_{\theta_z,k} + \varphi_3$$

where $m = -\frac{N-1}{2}, -\frac{N-3}{2}, ..., \frac{N-3}{2}$, $n = -\frac{N-1}{2}, -\frac{N-3}{2}, ..., \frac{N-1}{2}$, and $k = 1, 2, ..., K$.
It shall be pointed out that φ_0 and $\mathbf{t}_0 = [t_{0x}, t_{0y}]$ are the rotation and offset of the misalignment error of View 0 and the notations of other views are similar. And φ_0 is a small angle, for which the 'small angle' approximation can be adopted. For the rotation misalignment error of other views, this approximation is still tenable.

Similar to the presentation of [17], combining (5) and (11), summing over all the sites of (12) and (13), we can obtain the misalignment error, i.e. the offset components $t_{0x}, t_{0y}, t_{1x}, t_{1y}$, and the rotation components φ_0, φ_1, i.e.

$$t_{0x} = \frac{\sum_{m,n} V_{0,x,m,n}}{N^2}, \quad t_{0y} = \frac{\sum_{m,n} V_{0,y,m,n}}{N^2}$$

$$t_{1x} = \frac{\sum_{m,n} V_{1,x,m,n}}{N^2}, \quad t_{1y} = \frac{\sum_{m,n} V_{1,y,m,n}}{N^2}$$

$$\varphi_0 = \frac{\sum_{m,n} (V_{0,y,m,n} x_m - V_{0,x,m,n} y_n)}{\sum_{m,n} (x_m^2 + y_n^2)} \tag{16}$$

$$\varphi_1 = \frac{\sum_{m,n} (-V_{1,y,m,n} y_n - V_{1,x,m,n} x_m)}{\sum_{m,n} (x_m^2 + y_n^2)}$$

Noting Eqs. (5), (11), and (12), summing over all sites of (14) and (15), φ_2 and φ_3 can be determined, and the detailed result is

$$\varphi_2 = \frac{\sum_k V_{2,\theta_z,k} - \sum_k V_{0,\theta_z,k}}{K} + \frac{\sum_{m,n}\left(V_{0,y,m,n}x_m - V_{0,x,m,n}y_n\right)}{\sum_{m,n}\left(x_m^2 + y_n^2\right)}$$

$$\varphi_3 = \frac{\sum_k V_{3,\theta_z,k} - \sum_n V_{0,\theta_z,k}}{K} + \frac{\sum_{m,n}\left(V_{0,y,m,n}x_m - V_{0,x,m,n}y_n\right)}{\sum_{m,n}\left(x_m^2 + y_n^2\right)}$$

(17)

After elimination of the misalignment error in View 0, View 1, and View 2, combining Eq. (6), the measurement data are to be rearranged as:

$$U_{0,x,m,n} = V_{0,x,m,n} - t_{0x} + \varphi_0 y_n = F_{x,m,n} + A_{x,m,n} + Oy_n + Rx_m$$

$$U_{0,y,m,n} = V_{0,y,m,n} - t_{0y} - \varphi_0 x_m = F_{y,m,n} + A_{y,m,n} + Ox_m - Ry_n$$

(18)

$$U_{0,\theta_z,k} = V_{0,\theta_z,k} - \varphi_0 = G_{\theta_z,k} + A_{\theta_z,k}$$

$$U_{1,x,m,n} = V_{1,x,m,n} + \varphi_1 x_m - t_{1x} = F_{x,-n,m} - A_{y,m,n} + Ox_m - Ry_n$$

$$U_{1,y,m,n} = V_{1,y,m,n} + \varphi_1 y_n - t_{1y} = F_{y,-n,m} + A_{x,m,n} - Oy_n - Rx_m$$

(19)

$$U_{1,\theta_z,k} = V_{1,\theta_z,k} - \varphi_1 = G_{\theta_z,k+\frac{K}{4}} + A_{\theta_z,k}$$

$$U_{2,\theta_z,k} = V_{2,\theta_z,k} - \varphi_2 = G_{\theta_z,k+1} + A_{\theta_z,k}$$

(20)

And to keep the notation consistent with the previous views, we define

$$U_{3,x,m,n} = V_{3,x,m,n} + \varphi_3 y_n = F_{x,m+1,n} + A_{x,m,n} + Oy_n + Rx_m + \xi_x$$

$$U_{3,y,m,n} = V_{3,y,m,n} - \varphi_3 x_m = F_{y,m+1,n} + A_{y,m,n} + Ox_m - Ry_n + \xi_y$$

(21)

$$U_{3,\theta_z,k} = V_{3,y,m,n} - \varphi_3$$

where $\xi_x = t_{3x} + R\Delta$ and $\xi_y = t_{3y} + O\Delta$.

Comparing Eq. (18) of View 0 with Eq. (19) of View 1, with the same procedure in [17], the stage error components O and R can be calculated out as:

$$O = \frac{1}{2}\left[\frac{\sum_{m,n}\left(U_{0,x,m,n}y_n + U_{0,y,m,n}x_m\right)}{\sum_{m,n}\left(x_m^2 + y_n^2\right)} + \frac{\sum_{m,n}\left(U_{1,x,m,n}x_m - U_{1,y,m,n}y_n\right)}{\sum_{m,n}\left(x_m^2 + y_n^2\right)}\right]$$

$$R = \frac{1}{2}\left[\frac{\sum_{m,n}\left(U_{0,x,m,n}x_m - U_{0,y,m,n}y_n\right)}{\sum_{m,n}\left(x_m^2 + y_n^2\right)} + \frac{\sum_{m,n}\left(-U_{1,x,m,n}y_n - U_{1,y,m,n}x_m\right)}{\sum_{m,n}\left(x_m^2 + y_n^2\right)}\right]$$

(22)

3.2 XYθ$_z$ self-calibration algorithm

A least square-based self-calibration algorithm is synthesized to determinate $G_{m,n,k}$. In this algorithm, the computation of the misalignment error components ξ_x and ξ_y is unnecessary, while φ_3 is determined by Eq. (17). Because O and R are known by Eq. (22), the algorithm is constructed to just calculate out $F_{x,m,n}$, $F_{y,m,n}$, and $G_{\theta_z,k}$.

Comparing Eq. (18) with (19), one obtains

$$F_{x,m,n} - F_{y,-n,m} = U_{0,x,m,n} - U_{1,y,m,n} - 2Oy_n - 2Rx_m$$

$$F_{y,m,n} + F_{x,-n,m} = U_{0,y,m,n} + U_{1,x,m,n} - 2Ox_m + 2Ry_n$$

(23)

Then combining Eqs. (18) and (21), define

$$
\begin{aligned}
L_{x,m,n} &= U_{3,x,m,n} - U_{0,x,m,n} = F_{x,m+1,n} - F_{x,m,n} + \xi_x \\
L_{y,m,n} &= U_{3,y,m,n} - U_{0,y,m,n} = F_{y,m+1,n} - F_{y,m,n} + \xi_y
\end{aligned} \tag{24}
$$

Consequently, we can obtain

$$
\begin{aligned}
F_{x,m+2,n} - 2F_{x,m+1,n} + F_{x,m,n} &= L_{x,m+1,n} - L_{x,m,n} \\
F_{x,m+1,n+1} - F_{x,m+1,n} - F_{x,m,n+1} + F_{x,m,n} &= L_{x,m,n+1} - L_{x,m,n} \\
F_{y,m+2,n} - 2F_{y,m+1,n} + F_{y,m,n} &= L_{y,m+1,n} - L_{y,m,n} \\
F_{y,m+1,n+1} - F_{y,m+1,n} - F_{y,m,n+1} + F_{y,m,n} &= L_{y,m,n+1} - L_{y,m,n}
\end{aligned} \tag{25}
$$

From previous subsections, Eqs. (7), (23), and (25) can yield

$$
\begin{aligned}
\sum_{m,n} F_{x,m,n} &= \sum_{m,n} F_{x,m,n} x_m = \sum_{m,n} F_{x,m,n} y_n = 0 \\
\sum_{m,n} F_{y,m,n} &= \sum_{m,n} F_{y,m,n} x_m = \sum_{m,n} F_{y,m,n} y_n = 0 \\
F_{x,m,n} - F_{y,-n,m} &= U_{0,x,m,n} - U_{1,y,m,n} - 2Oy_n - 2Rx_m \\
F_{y,m,n} + F_{x,-n,m} &= U_{0,y,m,n} + U_{1,x,m,n} - 2Ox_m + 2Ry_n \\
F_{x,m+2,n} - 2F_{x,m+1,n} + F_{x,m,n} &= L_{x,m+1,n} - L_{x,m,n} \\
F_{x,m+1,n+1} - F_{x,m+1,n} - F_{x,m,n+1} + F_{x,m,n} &= L_{x,m,n+1} - L_{x,m,n} \\
F_{y,m+2,n} - 2F_{y,m+1,n} + F_{y,m,n} &= L_{y,m+1,n} - L_{y,m,n} \\
F_{y,m+1,n+1} - F_{y,m+1,n} - F_{y,m,n+1} + F_{y,m,n} &= L_{y,m,n+1} - L_{y,m,n}
\end{aligned} \tag{26}
$$

which actually can determinate $F_{x,m,n}$ and $F_{y,m,n}$ with certain redundancy. Then a least square estimation law for $F_{x,m,n}$ and $F_{y,m,n}$ can be synthesized through a least square solution of the set of $F_{x,m,n}$ and $F_{y,m,n}$ equations to meet the challenge of random measurement noise [17, 20, 21]. Thus, combining the solved parameters O and R, we can obtain $G_{x,m,n}$ and $G_{y,m,n}$.

Afterward, according to (9), we can obtain the determination of $G_{\theta_z,0}$, $G_{\theta_z,\frac{K}{4}}$, $G_{\theta_z,\frac{K}{2}}$, and $G_{\theta_z,\frac{3K}{4}}$ with certain redundancy. Here we use the method of least squares as follows:

$$
\begin{aligned}
G_{\theta_z,1} &= \frac{\sum_{m=1}^{M} G_{y,m,0} x_m - \frac{1}{M}\sum_{m=1}^{M} G_{y,m,0} \sum_{m=1}^{M} x_m}{\sum_{m=1}^{M} x_m^2 - \frac{1}{M}\left(\sum_{m=1}^{M} x_m\right)^2} \\[2em]
G_{\theta_z,1+\frac{K}{4}} &= -\frac{\sum_{n=1}^{M} G_{x,0,n} y_n - \frac{1}{M}\sum_{n=1}^{M} G_{x,0,n} \sum_{n=1}^{M} y_n}{\sum_{n=1}^{M} y_n^2 - \frac{1}{M}\left(\sum_{n=1}^{M} y_n\right)^2} \\[2em]
G_{\theta_z,1+\frac{K}{2}} &= \frac{\sum_{m=-M}^{-1} G_{y,m,0} x_m - \frac{1}{M}\sum_{m=-M}^{-1} G_{y,m,0} \sum_{m=-M}^{-1} x_m}{\sum_{m=-M}^{-1} x_m^2 - \frac{1}{M}\left(\sum_{m=-M}^{-1} x_m\right)^2} \\[2em]
G_{\theta_z,1+\frac{3K}{4}} &= -\frac{\sum_{n=-M}^{-1} G_{x,0,n} y_n - \frac{1}{M}\sum_{n=-M}^{-1} G_{x,0,n} \sum_{n=-M}^{-1} y_n}{\sum_{n=-M}^{-1} y_n^2 - \frac{1}{M}\left(\sum_{n=-M}^{-1} y_n\right)^2}
\end{aligned} \tag{27}
$$

where $M = \frac{N-1}{2}$. Noting Eqs. (18), (19), and (20), we consequently obtain

$$G_{\theta_z, k+\frac{K}{4}} - G_{\theta_z, k} = U_{1, \theta_z, k} - U_{0, \theta_z, k}$$

$$G_{\theta_z, k+1} - G_{\theta_z, k} = U_{2, \theta_z, k} - U_{0, \theta_z, k} \tag{28}$$

where $k = 1, 2, ..., K$ and $G_{\theta_z, k+K} = G_{\theta_z, k}$.

Combining (27) and (28), the stage error $G_{\theta_z, k}$ can be determined through a least square solution as the above equation group has K unknowns and $2K + 4$ equations.

The proposed method features certain benefits remarked as follows:

- In previous self-calibration schemes for *XY* stages and *XYZ* stages [17, 18, 20–23], the properties of no translation and no rotation for the stage error cannot be used in View 3. Resultantly, it needs complicated algebraic manipulations to determine the misalignment error component φ_3. In this chapter, Eq. (17) directly determines the value of φ_3, and it is so convenient that complicated algebraic manipulations are significantly avoided.

- We propose a new property to construct connection between *XY* orientation and θ_z orientation. By a least square method, values of $G_{\theta_z, 1}$, $G_{\theta_z, \frac{K}{4}}$, $G_{\theta_z, \frac{K}{2}}$, and $G_{\theta_z, \frac{3K}{4}}$ are determined by Eq. (27), which is quite important for the calculation algorithm of $G_{\theta_z, k}$. With full utilization of the measurement of View 0, View 1, and View 2, we can construct a simple algorithm with strong robustness.

4. Computer simulation

In this section, we use MATLAB software to simulate the self-calibration process. First, arbitrary stage linear error maps on a 11×11 sample site array with the sample site interval $\Delta = 10$ mm are generated using the command 'normrnd' with a mean of 0 and standard deviation of 0.2 μm, which are utilized as the nominal $G_{x, m, n}$ and $G_{y, m, n}$. Besides, any stage rotary error is mapped within a revolution, while the sample site internal is $\Delta = 15°$. And the nominal $G_{\theta_z, k}$ is generated by mean value of 0 and standard deviation of 0.01°. And minor modification has been made to the data to satisfy the relevant requirements like Eqs. (5), (9), and (11). Then, arbitrary artifact linear error maps are generated with mean of 0 and standard deviation of 0.3 μm, which are employed as the nominal $\mathbf{A}_{m, n}$, and arbitrary artifact rotary error maps are generated with a mean of 0 and standard deviation of 0.01°, which are utilized as the nominal $A_{\theta_z, k}$. The nominal stage error component $\mathbf{G}_{m, n}$ is shown in **Figure 4** where the red lines are $\mathbf{G}_{m, n} \times 10000$. The nominal stage error component $G_{\theta_z, k}$ is shown in **Figure 5** where $G_{\theta_z, k}$ between the actual measurement system and perfect measurement system has been zoomed in for $360/\pi$ times. In addition, for each view, we add a random misalignment which is made up of a rotation and an offset. And the standard deviation value in the misalignment is 0.3° for rotation and 30 μm for offset. Since Eq. (26) has some redundance, it is clear that $\mathbf{G}_{m, n, k}$ can be figured out rather accurately if there is no random measurement noise. In addition, as there are no reported complete on-axis $XY\theta_z$ self-calibration strategies in published papers, we just test their own effectiveness of the proposed strategy. Herein, we focus on testing the calibration accuracy of the proposed strategy in various random measurement noises.
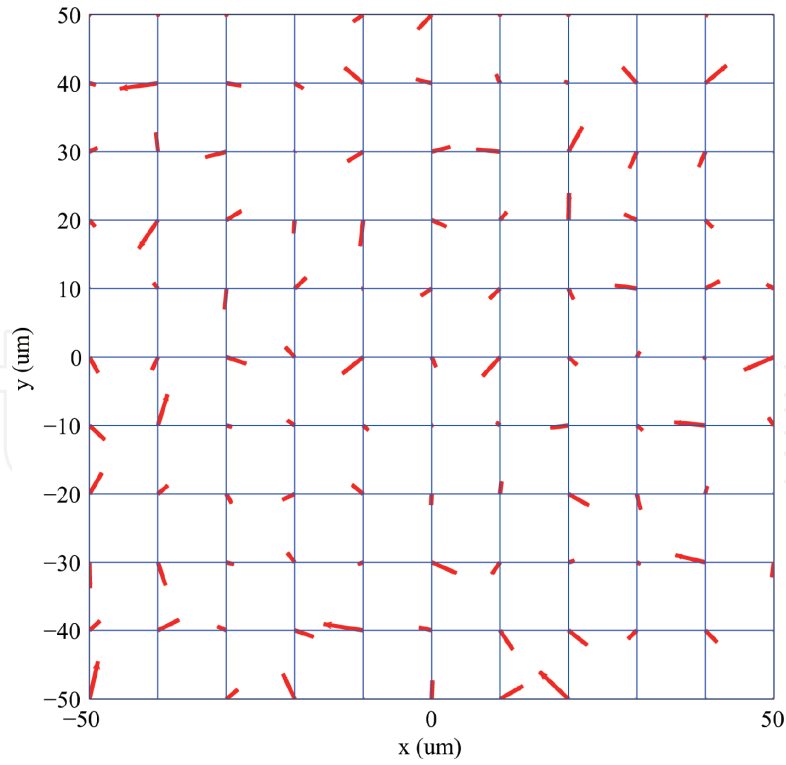
Figure 4.
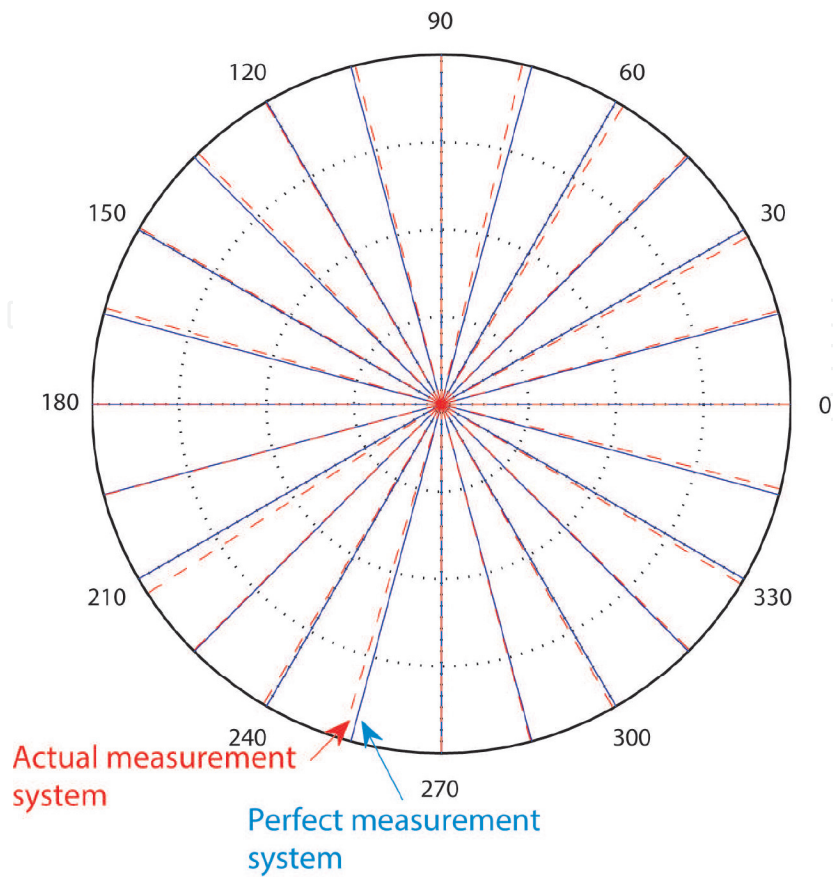*$G_{m,n} \times 10000$ with $max(G_{m,n}) = 0.5494\ \mu m$, $min(G_{m,n}) = -0.5806\ \mu m$.*

Actual measurement system

Perfect measurement system

Figure 5.
$G_{\theta_z,k} \times 360/\pi°$ with $max(G_{\theta_z,k}) = 0.0243°$, $min(G_{\theta_z,k}) = -0.01282°$.

4.1 Simulation with random measurement noise of standard deviation 0.02 μm for $G_{x,m,n}$ and $G_{y,m,n}$ and standard deviation 0.001° for $G_{\theta_z,k}$

For the simulation in this subsection, we add an independent random Gaussian measurement noise to every grid mark's each measurement and independent angular measurement noise to every angular mark's each measurement. $G_{x,m,n}$ and $G_{y,m,n}$'s random measurement noise is generated by a mean value 0 and standard deviation 0.02 μm, and $G_{\theta_z,k}$'s random measurement noise is generated by a mean value 0 and standard deviation 0.001°. The reconstructed stage error $\mathbf{G}_{m,n,k}$ can thus be determined according to the proposed four measurement views and self-calibration algorithm. So as to test the robustness of the algorithm, the calibration errors E_{Gx}, E_{Gy}, and $E_{G\theta}$ are calculated, which are defined as the deviation between the actual and the recalculated stage error, i.e. $E_{Gx} = G_{x,m,n} - \hat{G}_{x,m,n}$, $E_{Gy} = G_{y,m,n} - \hat{G}_{y,m,n}$, and $E_{G\theta} = G_{\theta,k} - \hat{G}_{\theta,k}$. In **Table 1**, the maximum, the minimum, and the standard deviation for E_{Gx}, E_{Gy}, and $E_{G\theta}$ are all listed. It is obvious that the stage error can be accurately recalculated by the proposed method even in the case of random measurement noise—when there is measurement noise by standard deviation 0.02 μm and 0.001° and the standard deviations of the calibration errors are smaller than 0.02 μm and 0.001°, respectively.

In addition, the algorithm's accuracy is also tested to meet the challenge of various random measurement noises. We generate the random measurement noises for 20 times. As a result, the calibration errors' standard deviations are shown in **Figures 6** and **7**. All the results illustrate that all the 20 standard deviations keep in the same level with the measurement noises themselves. The simulation results demonstrate that the algorithm is robust and accurate. In addition, it can deal with the challenge of random measurement noise effectively.

4.2 Simulation with random measurement noise of standard deviation 0.002 μm for $G_{x,m,n}$ and $G_{y,m,n}$ and standard deviation 0.0001° for $G_{\theta_z,k}$

The simulation in this subsection is set up exactly the same way as in the previous subsection, except for adding a different random Gaussian measurement noise to every site's measurement, which is to test the consistency of the proposed scheme's robustness to random measurement noise. The random measurement noise for $G_{x,m,n}$ and $G_{y,m,n}$ is generated with a mean of 0 and standard deviation of 0.002 μm, and the random measurement noise for $G_{\theta_z,k}$ is generated with a mean of 0 and standard deviation of 0.0001°. Through the proposed scheme, the reconstructed stage error $\mathbf{G}_{m,n,k}$ can be calculated out, and the maximum value $max(\cdot)$, the minimum value $min(\cdot)$, and the standard deviation $std(\cdot)$ of E_{Gx}, E_{Gy}, and $E_{G\theta}$ are detailed in **Table 2**. Furthermore, the algorithm's accuracy and robustness are tested for arbitrary 20 times; the results are shown in **Figures 8** and **9**. It can be observed that the calibration error is also about the same size as the random measurement noises themselves. All these results further verify that the proposed

	$max(\cdot)$	$min(\cdot)$	$std(\cdot)$
E_{Gx} (μm)	0.0541	−0.0490	0.0195
E_{Gy} (μm)	0.0511	−0.0506	0.0196
$E_{G\theta}$ (°)	1.5877e−003	−1.2065e−003	7.1184e−004

Table 1.
Calculation performance indexes (with random measurement noise std = 0.02 μM).
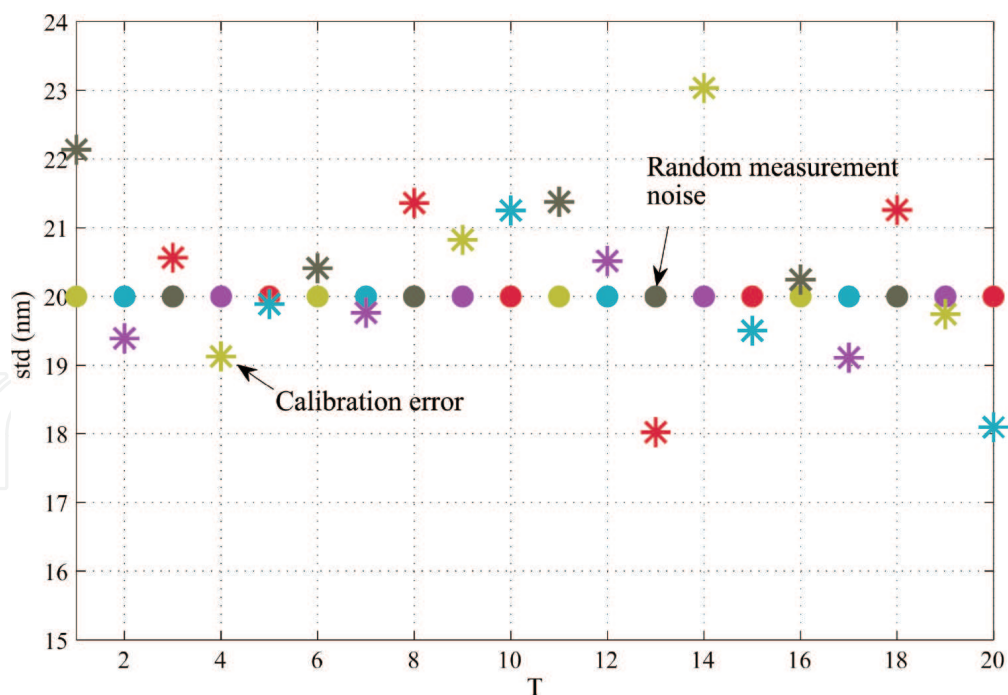
Figure 6.
Standard deviation of calibration error E_{Gx} & E_{Gy} for arbitrary 20 times (with random measurement noise std = 0.02 μm).
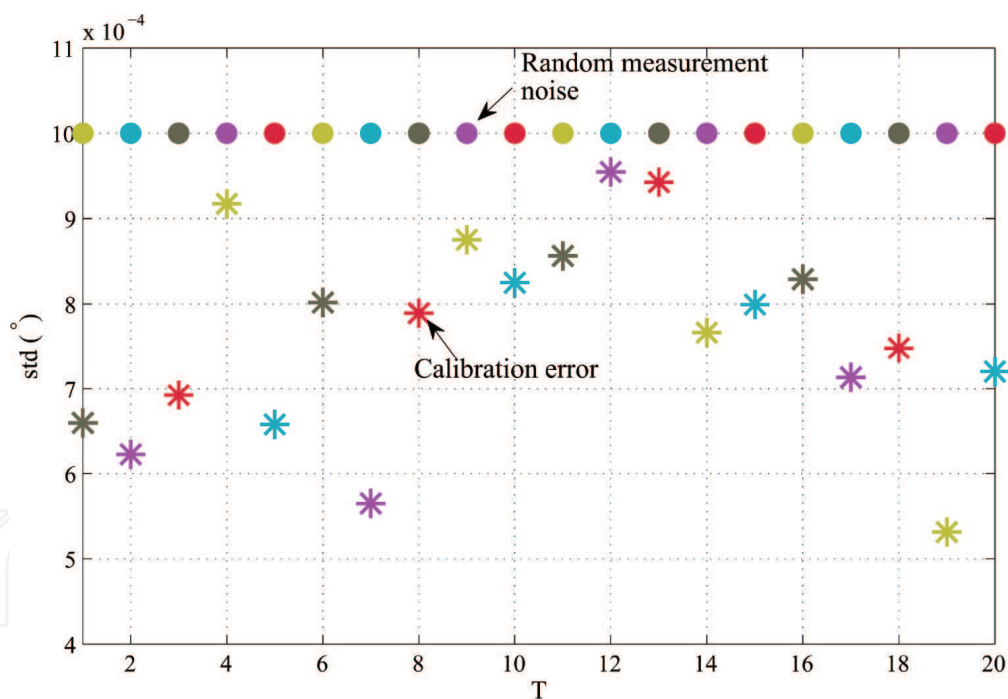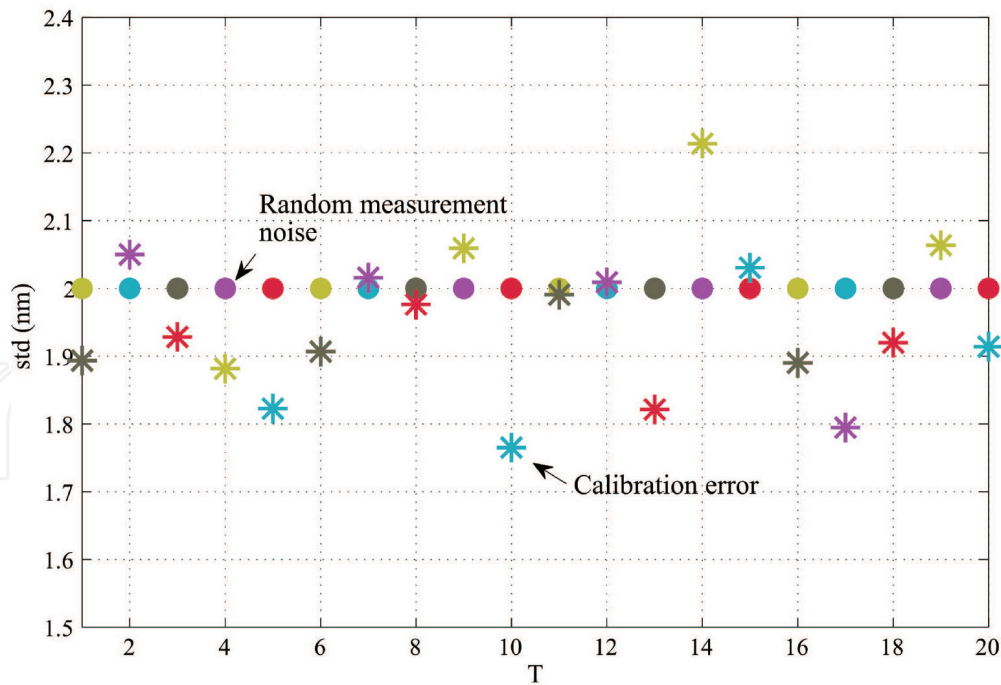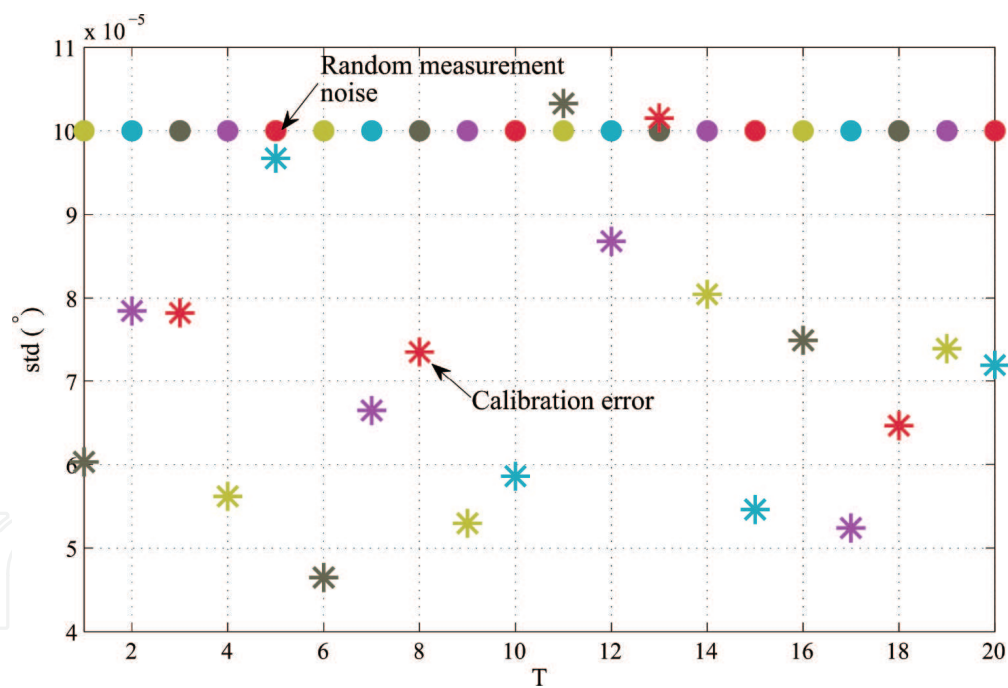

Figure 7.
Standard deviation of calibration error $E_{G\theta}$ for arbitrary 20 times (with random measurement noise std = 0.001°).

	$max(\cdot)$	$min(\cdot)$	$std(\cdot)$
E_{Gx} (μm)	0.0051	−0.0051	0.0020
E_{Gy} (μm)	0.0051	−0.0053	0.0020
$E_{G\theta}$ (°)	2.9963e−004	−6.9733e−004	7.6657e−005

Table 2.
Calculation performance indexes (with random measurement noise std = 0.02 μm).

Figure 8.
Standard deviation of calibration error E$_{Gx}$ & E$_{Gy}$ for arbitrary 10 times (with random measurement noise std = 0.002 μm).

Figure 9.
Standard deviation of calibration error E$_{Gθ}$ for arbitrary 20 times (with random measurement noise std = 0.0001°).

strategy can accurately determine the stage error even under the existence of random measurement noise.

4.3 The artifact plate and the procedure for performing a standard $XYθ_z$ self-calibration

Based on the proposed theory principle, we design and manufacture an artifact plate for $XYθ_z$ self-calibration. The specification of the practical artifact plate is shown in **Figure 10**. Specifically, the artifact plate is made in square shape with
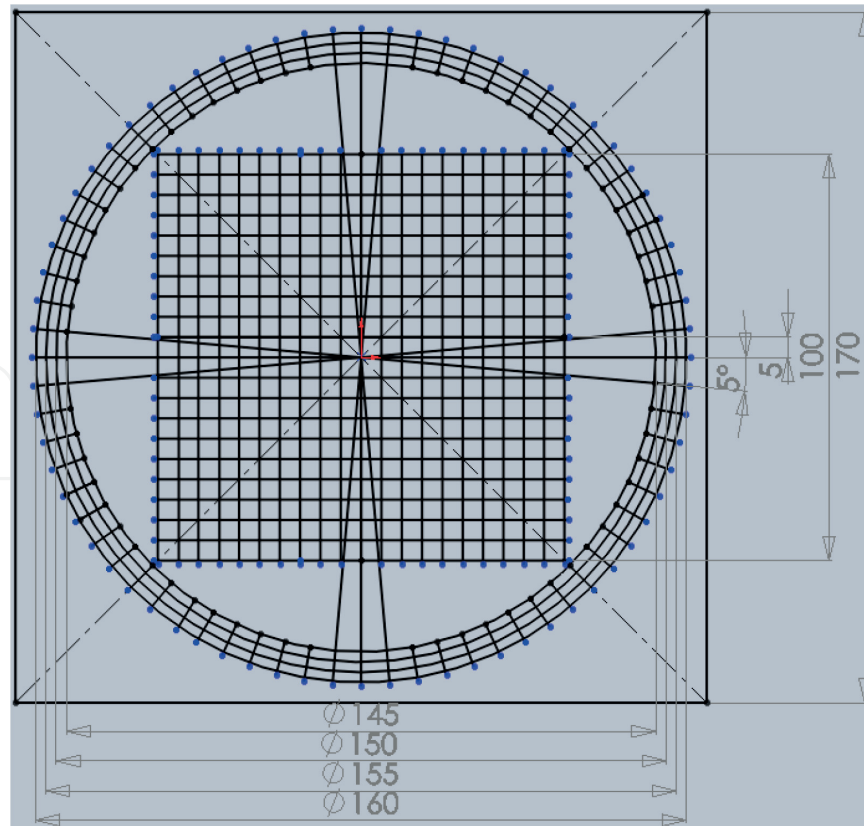
Figure 10.
A designed artifact plate for XYθ$_z$ self-calibration.

material of optical glass. The thickness is 3 mm. The origin of the plate is located at the center. The radius or the circle in the plate is 80 mm. The circle of 360° is divided into 72 sectors by 72 lines with a width of 5 μm and accuracy of 5". The 21 × 21 sample site array is with the sample site interval Δ = 5 mm. The accuracy of the circle lines and the straight lines is ±1 μm and the width is 5 μm.

For presentation, convenience, and clarity, an example of an artifact plate on a *XYθ$_z$* stage is also provided and shown in **Figure 11**. In the following, we list the procedure of performing a standard *XYθ$_z$* self-calibration following the proposed scheme, which may be useful for engineers in practical implementations:

Step 0: As shown in **Figures 3** and **11**, put the artifact plate shown in **Figure 10** in the *XYθ$_z$* stage. The artifact plate's array marks are consequently at the stage's origin
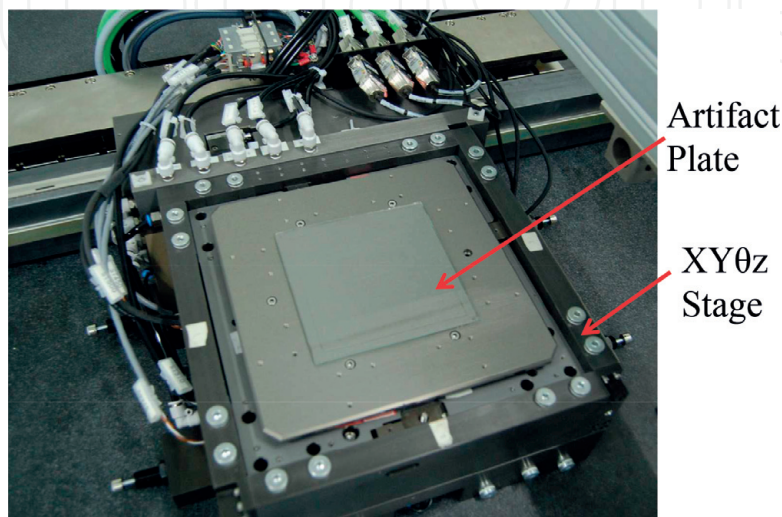

Figure 11.
An artifact plate on a XYθ$_z$ stage for self-calibration.

reference location, which is named as View 0 of **Figure 3**. The artifact plate's mark locations are measured in the $XY\theta_z$ metrology stage with the help of some mark alignment system such as those in [21, 23]. The mark alignment system should be designed to obtain the measurement data of each mark position accurately. Get $V_{0,x,m,n}$, $V_{0,y,m,n}$, and $V_{0,\theta_z,k}$ for P (e.g. $P = 5$) times, and average the results, and then obtain $U_{0,x,m,n}$, $U_{0,y,m,n}$, and $U_{0,\theta_z,k}$ by Eq. (18).

Step 1: After rotating 90° around the origin shown as View 1 in **Figure 3**, the artifact plate is replaced to the rotated reference location on the stage. The $XY\theta_z$ metrology stage is utilized to measure the artifact plate mark locations. Obtain $V_{1,x,m,n}$, $V_{1,y,m,n}$, and $V_{1,\theta_z,k}$ for P (e.g. $P = 5$) times and average the results. Get $U_{1,x,m,n}$, $U_{1,y,m,n}$, and $U_{1,\theta_z,k}$ by Eq. (19). And calculate out O and R by Eq. (22).

Step 2: After rotating $360/K°$ around the origin shown as View 2 in **Figure 3**, the artifact plate is replaced to the rotated reference location in the stage. The $XY\theta_z$ metrology stage is utilized to measure the angles of the artifact plate mark lines, and get $V_{2,\theta_z,k}$ for P (e.g. $P = 5$) times, and average the results, and then obtain $U_{2,\theta_z,k}$ by Eq. (20).

Step 3: After translating one grid interval Δ along +X-axis of the stage shown as View 3 in **Figure 3**, the artifact plate is replaced to the translated reference location in the stage. The $XY\theta_z$ metrology stage is used to measure the location of the marks of the artifact plate, and get $V_{3,x,m,n}$, $V_{3,y,m,n}$, and $V_{3,\theta_z,k}$ for P (e.g. $P = 5$) times, and average the results. Obtain $U_{3,x,m,n}$, $U_{3,y,m,n}$, and $U_{3,\theta_z,k}$ by Eq. (21).

Step 4: After above steps, the equation groups (26), (27), and (28) can be obtained. Therefore, a least square solution can be used for the determination of $F_{x,m,n}$, $F_{y,m,n}$, and $G_{\theta_z,k}$. Then $G_{x,m,n}$ and $G_{y,m,n}$ can be determined by Eq. (6) as O and R are previously computed in Step 1, which completes the final determination of $\mathbf{G}_{m,n,k}$.

5. Conclusions

In this chapter, an on-axis self-calibration approach has been first developed for precision $XY\theta_z$ metrology stages to solve the calibration problem. The proposed scheme uses a new artifact plate designed with special mark lines as the assistant tool for calibration. In detail, the artifact plate is placed on the uncalibrated $XY\theta_z$ metrology stages in four measurement postures or views. Then, the measurement error can be modeled as the construction of $XY\theta_z$ systematic measurement error (i.e. stage error) and other errors or noise. Based on the redundance of the $XY\theta_z$ stage error, a least square-based $XY\theta_z$ self-calibration law is resultantly synthesized for final determination of the stage error. Computer simulations have been conducted to verify that the proposed method can figure out the stage error rather accurately even under existence of various random measurement noises. Finally, a standard on-axis $XY\theta_z$ self-calibration procedure with the designed artifact plate is introduced. As an integration of XY self-calibration and θ self-calibration, the proposed scheme solves the $XY\theta_z$ self-calibration problem without complicated mathematical processing for misalignment errors. The developed approach has essentially provided a fundamental principle for on-axis self-calibration of precision $XY\theta_z$ metrology stages in practical applications.

The proposed scheme has pros and cons. It provides a significant theory fundamental for self-calibration of $XY\theta_z$ metrology or motion stages. However, the calibration accuracy is seriously affected by the mark alignment systems which may be a little complex. Therefore, the proposed self-calibration scheme is very suitable for standard calibration in national standard institutes but a little limited for wide

industrial applications. In the next step, the development of this calibration system is an important topic, which will do help for wide applications of the proposed scheme.

Acknowledgements

Author details

Chuxiong Hu[1,2*], Yu Zhu[1,2] and Luzheng Liu[1,2]

1 State Key Lab of Tribology, Department of Mechanical Engineering, Tsinghua University, Beijing, China

2 Beijing Key Lab of Precision/Ultra Precision Manufacture Equipments and Control, Tsinghua University, Beijing, China

*Address all correspondence to: cxhu@tsinghua.edu.cn

IntechOpen

References

[1] Zhong G, Shao Z, Deng H, Ren J. Precise position synchronous control for multi-axis servo systems. IEEE Transactions on Industrial Electronics. 2017;**64**(5):3707-3717

[2] Hu C, Wang Z, Zhu Y, et al. Accurate three-dimensional contouring error estimation and compensation scheme with zero-phase filter. International Journal of Machine Tools and Manufacture. 2018;**128**:33-40

[3] Hu C, Hu Z, Zhu Y, Wang Z. Advanced GTCF based LARC contouring motion control on an industrial X-Y linear-motor-driven stage with experimental investigation. IEEE Transactions on Industrial Electronics. 2017;**64**(4):3308-3318

[4] Chen Z, Yao B, Wang Q. μ-Synthesis based adaptive robust control of linear motor driven stages with high-frequency dynamics: A case study with comparative experiments. IEEE/ASME Transactions on Mechatronics. 2015;**20**(3):1482-1490

[5] Chen Z, Yao B, Wang Q. Accurate motion control of linear motors with adaptive robust compensation of nonlinear electromagnetic field effect. IEEE/ASME Transactions on Mechatronics. 2013;**18**(3):1122-1129

[6] Hu C, Wang Z, Zhu Y, Zhang M, Liu H. Performance oriented precision LARC tracking motion control of a magnetically levitated planar motor with comparative experiments. IEEE Transactions on Industrial Electronics. 2016;**63**(9):5763-5773

[7] Liu G, Dass R, Nguang S-K, Partridge A. Principles, design, and calibration for a genre of irradiation angle sensors. IEEE Transactions on Industrial Electronics. 2013;**60**(1): 210-216

[8] Li X, Shamsi P. Model predictive current control of switched reluctance motors with inductance auto-calibration. IEEE Transactions on Industrial Electronics. 2016;**63**(6): 3934-3941

[9] Evans CJ, Hocken RJ, Estler WT. Self-calibration: Reversal, redundancy, error separation, and 'absolute testing. Annals of the CIRP. 1996;**35**(2):617-632

[10] Zhao Y, Lin Y, Xi F. Calibration-based iterative learning control for path tracking of industrial robots. IEEE Transactions on Industrial Electronics. 2015;**62**(5):2921-2929

[11] Takac MT, Ye J, Raugh MR, et al. Self-calibration in two dimensions: The experiment. In: Proceedings of SPIE Metrology, Inspection, and Process Control for Microlithog.; Bellingham. 1996. pp. 130-146

[12] Raugh MR. Two-dimensional stage self-calibration: Role of symmetry and invariant sets of points. Journal of Vacuum Science & Technology B. 1997;**15**(6):2139-2145

[13] De Cecco M, Debei S, Zaccariotto M, et al. A self-calibration method for nonorthogonal angles between gimbals of rotational inertial navigation system. IEEE Transactions on Industrial Electronics. Nov. 2015;**62**(4):2352-2362

[14] Lu X-D, Trumper DL. Self-calibration of on-axis rotary encoders. CIRP Annals: Manufacturing Technology. 2007;**56**(1):499-504

[15] Takac MT. Self-calibration in one dimension. In: Proceedings of SPIE 13th Annual BACUS Symposium on Photomask Technology and Management; Santa Clara. 1993. pp. 80-86

[16] Jeong YH, Dong J, Ferreira PM. Self-calibration of dual-actuated single-axis nanopositioners. Measurement Science and Technology. 2008;**19**(4):1-13

[17] Ye J, Takac MT, Berglund CN, et al. An exact algorithm for self-calibration of precision metrology stages. Precision Engineering. 1997;**20**(1):16-32

[18] Yoo S, Kim SW. Self-calibration algorithm for testing out-of-plane errors of two-dimensional profiling stages. International Journal of Machine Tools & Manufacture. 2004;**44**:767-774

[19] Xu M, Dziomba T, Dai G, Koenders L. Self-calibration of scanning probe microscope: Mapping the errors of the instrument. Measurement Science and Technology. 2008;**19**(2):1-6

[20] Hu C, Zhu Y, Hu J, Zhang M, Xu D. A holistic self-calibration algorithm for XY precision metrology systems. IEEE Transactions on Instrumentation and Measurement. 2012;**61**(9):2492-2500

[21] Zhu Y, Hu C, Hu J, Yang K. Accuracy and simplicity oriented self-calibration approach for two-dimensional precision stages. IEEE Transactions on Industrial Electronics. 2012;**60**(6):2264-2272

[22] Dang QC, Yoo S, Kim S-W. Complete 3-D self-calibration of coordinate measuring machines. Annals of the CIRP. 2006;**55**(1):1-4

[23] Hu C, Zhu Y, Hu J, Xu D, Zhang M. A holistic self-calibration approach for determination of three-dimensional stage error. IEEE Transactions on Instrumentation and Measurement. 2013;**62**(2):483-494

[24] Lu X-D, Graetz R, Amin-Shahidi D, Smeds K. On-axis self-calibration of angle encoders. CIRP Annals: Manufacturing Technology. 2010;**59**(1): 529-534

[25] Estler T, Queen H. An advanced angle metrology system. Annals of the CIRP. 1993;**42**(1):573-576

[26] Estler WT. Uncertainty analysis for angle calibrations using circle closure. Journal of Research of the National Institute of Standards and Technology. 1998;**103**(2):141-151

[27] Masuda T, Kajitani M. An automatic calibration system for angular encoders. Precision Engineering. 1989;**11**(2): 95-100

[28] Watanabe T, Fujimoto H, Masuda T. Self-calibratable rotary encoder. In: Proceedings of the 7th Int., Sym, Meas., Techol. Intellig. Instrum. 2005. pp. 240-245

[29] Kim J-A, Kim JW, Kang C-S, Jin J, Eom TB. Precision angle comparator using self-calibration of scale errors based on the equal-division-averaged method. In: MacroScale 2011 – Proceedings. Recent Developments in Traceable Dimensional Measurements. 2011. pp. 1-4

[30] Probst R. Self-calibratable of divided circles on the basis of a prime factor algorithm. Measurement Science and Technology. 2008;**19**(1):1-11

[31] Just A, Krause M, Probst R, Bosse H, Haunerdinger H, Spaeth C, et al. Comparison of angle standards with the aid of a high-resolution angle encoder. Precision Engineering. 2009;**33**:530-533

[32] Zhu Y, Hu C, Hu J, Zhang M, Xu D. On-axis self-calibration of precision $XY\theta_z$ metrology systems: An approach framework. In: Proceedings of 2013 IEEE/ASME International Conference on Advanced Intelligent Mechatronics (AIM). 2013. pp. 1078-1083